First-principles study on lithium metal borate cathodes for lithium rechargeable batteries

Dong-Hwa Seo (서동화),[1,2] Young-Uk Park (박영욱),[1] Sung-Wook Kim (김성욱),[1] Inchul Park (박인철),[3] R. A. Shakoor,[3] and Kisuk Kang (강기석)[1,*]

[1]*Department of Materials Science and Engineering, Seoul National University, 599 Gwanak-ro, Gwanak-gu, Seoul 151-742, Republic of Korea*

[2]*Department of Materials Science and Engineering, KAIST, 291 Daehak-ro, Yuseong-gu, Daejeon 305-701, Republic of Korea*

[3]*Graduate School of Energy, Environment, Water, and Sustainability, KAIST, 291 Daehak-ro, Yuseong-gu, Daejeon 305-701, Republic of Korea*

(Received 3 November 2010; revised manuscript received 17 March 2011; published 25 May 2011)

A computational study of the electrochemical properties of three isotopic $LiMBO_3$ compounds (M = Mn, Fe, and Co) as cathode materials is conducted using state-of-the-art first-principles calculations. The calculation of the Li intercalation potentials of $LiMBO_3$ predicts that the theoretical energy density (660–860 Wh kg^{-1}) can be comparable to or even higher than the corresponding olivine phosphates (595 Wh kg^{-1} for $LiFePO_4$). In addition, the volume changes during cycling are notably low (less than 2% for M = Mn, Fe, and Co), which may be advantageous for the long-term cyclability of Li rechargeable batteries. An investigation of the electronic structure suggests that the small polaron is likely to be a main conductor of Li_xMBO_3. A study of Li mobility in Li_xMBO_3 crystal structures indicates that zigzag one-dimensional (1D) Li diffusion tunnels are present with reasonably low activation barriers for Li motion. However, relatively low antisite energy for Li-M site exchange is observed, indicating that the metal ions in the Li site can block the 1D Li diffusion path. This implies that the synthesis condition and nanosizing of the material can be critical for this class of electrode material to achieve high-power capability.

DOI: 10.1103/PhysRevB.83.205127 PACS number(s): 82.47.Aa, 31.15.A−, 66.30.−h

I. INTRODUCTION

Polyanion-based materials such as phosphates,[1–9] silicates,[10–12] fluorophosphates and fluorosulfates[13,14] and borates[15–19] have been proposed as promising cathodes for Li rechargeable batteries. The variety of combinations between polyanions and transition metals (TMs) enables the tuning of electrochemical properties of this class of materials. It has been demonstrated that Li intercalation potentials (inductive effect),[1,2,11,20] Li storage capacity (variety of crystal structures and molecular weight of polyanions), thermal stability (oxygen chemical potential),[21,22] and other factors are critically dependent on the species of polyanion.

Regarding this group of polyanion materials, Legagneur *et al*. first reported the electrochemical properties of $LiMBO_3$ (M = Mn, Fe, and Co) as cathodes of a Li rechargeable battery.[15] In their report, $LiMBO_3$ cathodes could deliver only limited capacities even at slow rates of charge or discharge (about 9 mAh g^{-1} at C/250 for $LiFeBO_3$). The low capacity of $LiMBO_3$ was attributed to exceptionally large polarization. However, recently Abouimrane *et al*. applied carbon nanopainting on $LiFeBO_3$ and demonstrated that a large capacity of 158 mAh g^{-1} can be obtained from $LiFeBO_3$ at C/20 and 80 °C.[16] More recently, Yamada *et al*. showed that the theoretical capacity of $LiFeBO_3$ can nearly be achieved under moderate current density at room temperature by nanosizing and avoiding surface poisoning.[18] In particular, it was demonstrated that the extremely high polarization of $LiFeBO_3$ is caused partially by surface poisoning. This series of works presents new possibilities for the development of cathodes made with lithium metal borates that have both high energy density and stability.

In this paper, we investigate the intrinsic structural, electronic, and electrochemical properties of lithium metal borates using first-principles calculations. A comparative study of $LiMBO_3$ (M = Mn, Fe, and Co) is performed under this framework. We believe the fundamental study presented here can broaden the understanding of this new class of materials and provide insights to optimize them for a better-performing Li rechargeable battery.

II. COMPUTATIONAL DETAILS

The first-principles calculations were conducted with the spin-polarized generalized gradient approximation (GGA), using the Perdew–Burke–Ernzerhof exchange-correlation parametrization to the density functional theory (DFT).[23] A plane-wave basis set and the projector-augmented-wave (PAW) method were used as implemented in the Vienna *ab initio* simulation package (VASP).[24] PAW potentials have been widely used for battery materials and have shown good predictive capability.[25–30]

However, incomplete cancellation of the self-interaction of the GGA or the local density approximation (LDA) is often reported to result in large errors, especially for systems with strong localization of the metal *d* orbitals, such as phosphate materials.[26,27,31] The GGA+U approach[32,33] was therefore used to accurately calculate structural and electronic properties. We employed the rotationally invariant scheme for GGA+U as presented by Anisimov *et al*.[33] U values for Mn, Fe, and Co ions in borates have not yet been reported. However, the self-consistently calculated U values of olivine phosphates (U_P) were previously determined and are adopted here as reference U values for the calculation (Mn, 4.5 eV; Fe, 4.3 eV;

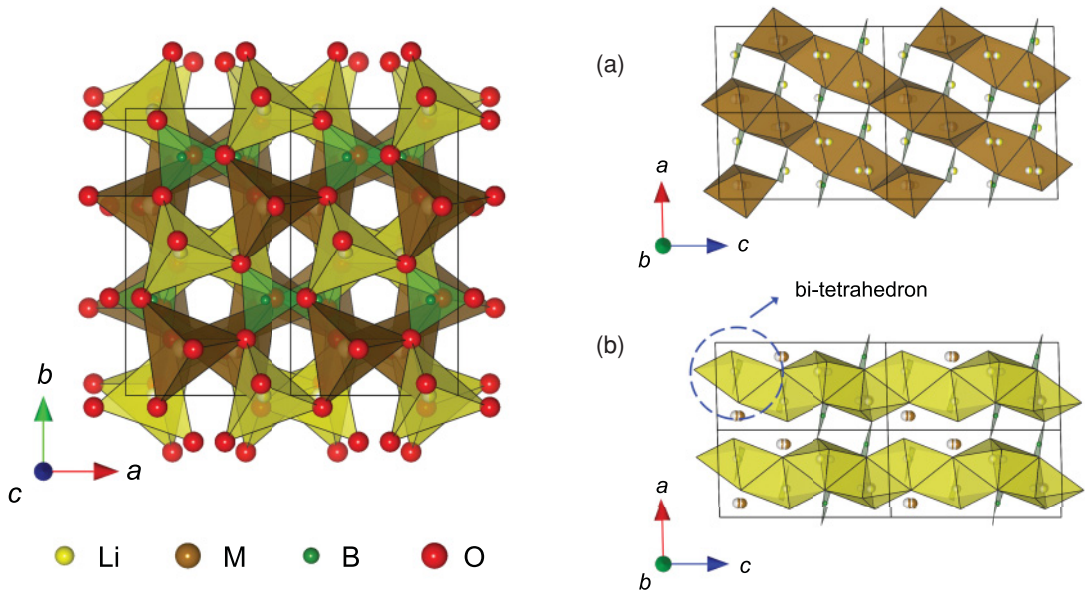

FIG. 1. (Color online) The structure of $LiMBO_3$ (M = Mn, Fe, and Co): (a) MO_5 chains with edge-sharing along the [−101] direction, and (b) edge-shared chains of LiO_4 parallel to the [001] direction.

Co, 5.7 eV). Since electrons can be less localized around TM ions in borates than those in phosphates and since orbitals of TM ions in borates are likely to be more overlapped than those in olivine due to shorter TM-TM distances, we also performed the calculations with slightly lower U values. U_P, $U_P - 0.3$ eV, and $U_P - 0.6$ eV were used as U values for Li_xMBO_3 ($x = 1$ and 0, M = Mn, Fe, and Co). Unless specifically mentioned, the results were similar for these U values tested. The estimation of the activation barrier for Li mobility was done within the GGA scheme without U to compare with the reported values in olivine, spinel, and layered structures.[34–36] All calculations were performed in supercells ($2a \times b \times c$) of eight formula units of Li_xMBO_3 (M = Mn, Fe, Co) at $x = 1$ and $x = 0$. A plane-wave basis with a kinetic energy cutoff of 500 eV was used, and reciprocal-space k-point meshes of $3 \times 3 \times 3$ were used to ensure that the total energies were converged within 5 meV per formula unit.

Activation barriers for the Li mobility in Li_xMBO_3 are calculated with the nudged-elastic-band (NEB) method in supercells ($2a \times b \times c$).[37] For these calculations, a Li ion is allowed to diffuse in the supercell of $Li_{15/16}MBO_3$ (M = Mn, Fe, Co). The NEB method is used with five replicas of the systems, which are initiated by linear interpolation between the initial and final states of the path.[38] All lattice parameters are fixed at $x = 1$, but all the internal degrees of freedom are relaxed during NEB calculation.

III. RESULTS AND DISCUSSION

A. Crystal structure

$LiMnBO_3$, $LiFeBO_3$, and $LiCoBO_3$ all adopt similar monoclinic crystal structures as a ground-state structure (a hexagonal polymorph does exist for $LiMnBO_3$ as a high-temperature phase experimentally).[15] Figure 1 shows the schematic crystal structure of $LiMBO_3$ (M = Mn, Fe, and Co) in c2/c monoclinic unit cells with four formula units.[15,17,18,39,40] TM ions occupy trigonal bipyramidal sites and slightly shift off the centers of these sites. This asymmetric coordination makes two different crystallographic sites for TM ions, M1 and M2 sites. The distances between the M1 and M2 sites are so small, at about 0.3 Å, that adjacent M1 and M2 sites cannot be simultaneously occupied. Each MO_5 hexahedron edge-shares with the neighboring MO_5; thus, they make the chains that run along [−101] [Fig. 1(a)]. Li ions are surrounded by four oxygen ions and occupy two different sites, Li1 and Li2 sites, whose occupancies are 0.5 for both sites. Li1 and Li2 tetrahedrons face-share with each other and form bitetrahedron units [Fig. 1(b)]. These bitetrahedron units are connected with others by edge-sharing and corner-sharing along [001] to make a one-dimensional (1D) Li diffusion pathway. Details of the Li diffusion in this crystal structure will be discussed in a later section. Two kinds of chains, MO_5 and LiO_4, are interconnected by corner-sharing with planar BO_3 units as shown in a projected ab plane of $LiMBO_3$ (Fig. 1).

TABLE I. Calculated and experimental lattice parameters of $LiMBO_3$ (M = Mn, Fe, and Co). ΔV indicates volume change between $LiMBO_3$ and MBO_3.

	a (Å)	b (Å)	c (Å)	β (deg.)	ΔV
$LiMnBO_3$	5.225	9.013	10.446	91.82	2.0%
$MnBO_3$	5.249	8.971	10.135	91.11	
exp-$LiMnBO_3$ (Ref. 40)	5.19	8.95	10.37	91.80	
$LiFeBO_3$	5.230	9.024	10.236	91.36	1.4%
$FeBO_3$	5.241	8.957	10.150	90.92	
exp-$LiFeBO_3$ (Ref. 18)	5.16	8.92	10.19	91.36	
$LiCoBO_3$	5.164	8.898	10.189	91.41	1.6%
$CoBO_3$	5.199	8.852	10.005	90.24	
exp-$LiCoBO_3$ (Ref. 39)	5.13	8.84	10.10	91.36	

Calculated lattice parameters of Li_xMBO_3 (M = Mn, Fe, Co) at $x = 1$ and $x = 0$ are tabulated in Table I. The lattice parameters of lithiated phases are in agreement with reported experimental values within 2%.[15,17,18,39,40] Although experimental results for fully delithiated states have not yet been reported, we predict those lattice parameters in Table I. For delithiated phases, b and c decrease, in general, while a slightly increases compared with $LiMBO_3$ (M = Mn, Fe, Co). For $LiFeBO_3$ and $LiCoBO_3$, the change of lattice parameters is nearly negligible with delithiation, whereas a slightly larger lattice parameter change is observed for $LiMnBO_3$. The change of c in Li_xMnBO_3 is particularly noteworthy. This seems to be correlated with the electronic configuration of Mn in the structure and will be discussed in the following section. Nevertheless, the overall volume change before and after delithiation is remarkably small for this class of materials. The volume change is only 1.4% for Li_xFeBO_3, 1.6% for Li_xCoBO_3, and 2.0% for Li_xMnBO_3. This is in clear contrast to other cathode materials, such as $LiFePO_4$ (6.5%), $LiMnPO_4$ (9.1%), and $LiMn_2O_4$(6.4%).[26,41] Small structural changes with deintercalation or intercalation may facilitate lithium motion in the structure and promote a reversible reaction, promising good cycle life for Li_xMBO_3 (M = Mn, Fe, Co). Indeed, Yamada *et al.* in their recent experiments demonstrated that Li_xFeBO_3 can exhibit excellent cyclability with only 2% volume change ($0.15 \leqslant x \leqslant 1$).[18]

B. Electronic structure

The electronic structures of lithium metal borates are studied in this chapter. First, an analysis on the spin density and total density of states (DOS) of Li_xMBO_3 (M = Mn, Fe, Co) at $x = 1$ and $x = 0$ is conducted. Table II shows the integrated spin density within the Voronoi volume of each TM ion. This is comparable to a plateau value when the integrated spin density is plotted with a distance from a TM ion core in Li_xMBO_3 (M = Mn, Fe, Co).[5,42] The calculated net moments are +4.77, +3.79, and +2.85 for Mn, Fe, and Co in $LiMBO_3$ (M = Mn, Fe, Co) with U_P, respectively. No significant change was observed for other U values ($U_P - 0.3$ eV and $U_P - 0.6$ eV). These net moments agree well with the unpaired electron spin counts of Mn^{2+}(+5), Fe^{2+}(+4), and Co^{2+}(+3) in high-spin states, respectively.[5,43] Typically the net moments are slightly underestimated in the computation, which is commonly observed in olivine and layered structures due to the transfer of the moment of oxygen ions.[5,43] Net moments are observed to decrease to +3.98, +4.32, and +3.23 for Mn, Fe, and Co in delithiated states, MBO_3 (M = Mn, Fe, Co), respectively. These are also close to the unpaired electron spin counts of Mn^{3+}(+4), Fe^{3+}(+5), and Co^{3+} (+4) in high-spin states.

TABLE II. Electronic structures of Li_xMBO_3 ($x = 1$ and 0, M = Mn, Fe, and Co).

	Electron configuration	Net moment (1/2 μB)	Bandgap (eV)
$LiMnBO_3$	$e''^2\, e'^2\, a'^1$	4.77	3.15
$MnBO_3$	$e''^2\, e'^2\, a'^0$	3.98	0.49
$LiFeBO_3$	$e''^3\, e'^2\, a'^1$	3.79	3.19
$FeBO_3$	$e''^2\, e'^2\, a'^1$	4.32	1.59
$LiCoBO_3$	$e''^4\, e'^2\, a'^1$	2.85	3.26
$CoBO_3$	$e''^3\, e'^2\, a'^1$	3.23	0.76

Electron configurations of Li_xMBO_3 (M = Mn, Fe, Co) at $x = 1$ and $x = 0$ are estimated considering the calculated net moments and DOS, as shown in Table II. Because the TM ions of Li_xMBO_3 occupy trigonal bipyramidal sites surrounded by five oxygen ions, the 3d bands of TM ions are split into the e'' (d_{xz}, d_{yz}), e' (d_{xy}, $d_{x^2-y^2}$), and a' (d_{z^2}) bands by crystal-field theory.[44] Figure 2(a) illustrates the schematic energy splitting of the MO_5 trigonal bipyramid. Considering the band splitting and the calculated net moments, Figure 2(b) shows that $LiMnBO_3$ has five up-spin electrons which occupy the e'', e', and a' bands at high-spin states. Thus the highest occupied band is the a' band for up-spin electrons and the lowest unoccupied band is e'' for down-spin electron in DOS, as shown in Fig. 3(a). Since an electron will be extracted from the a' band of $LiMnBO_3$ with the removal of an Li ion, the electronic configuration of $MnBO_3$ will be with the highest occupied band (e') and the lowest unoccupied band (a') for up-spin electrons, as shown in Fig. 3(b). For $LiFeBO_3$, Figure 2(b) reveals that five up-spin electrons

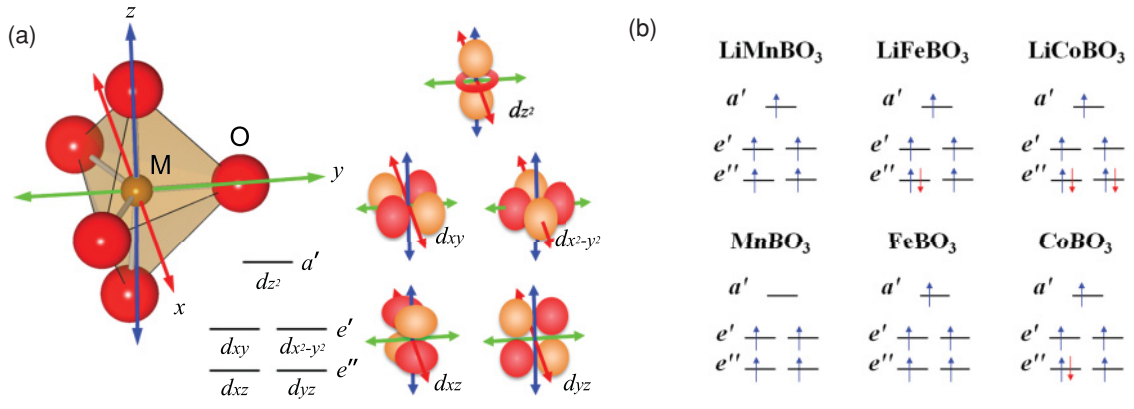

FIG. 2. (Color online) (a) MO_5 trigonal bipyramid and schematic energy levels of the 3d bands of the TM ion in trigonal bipyramidal coordination, and (b) schematic energy levels and occupied electrons of Li_xMBO_3 ($x = 1$, 0, M = Mn, Fe, Co). The 3d bands are split into the e'' (d_xz, d_yz), e' (d_xy, $d_{x^2-y^2}$), and a' (d_{z^2}) bands by the electrostatic field generated by five oxygen ions.

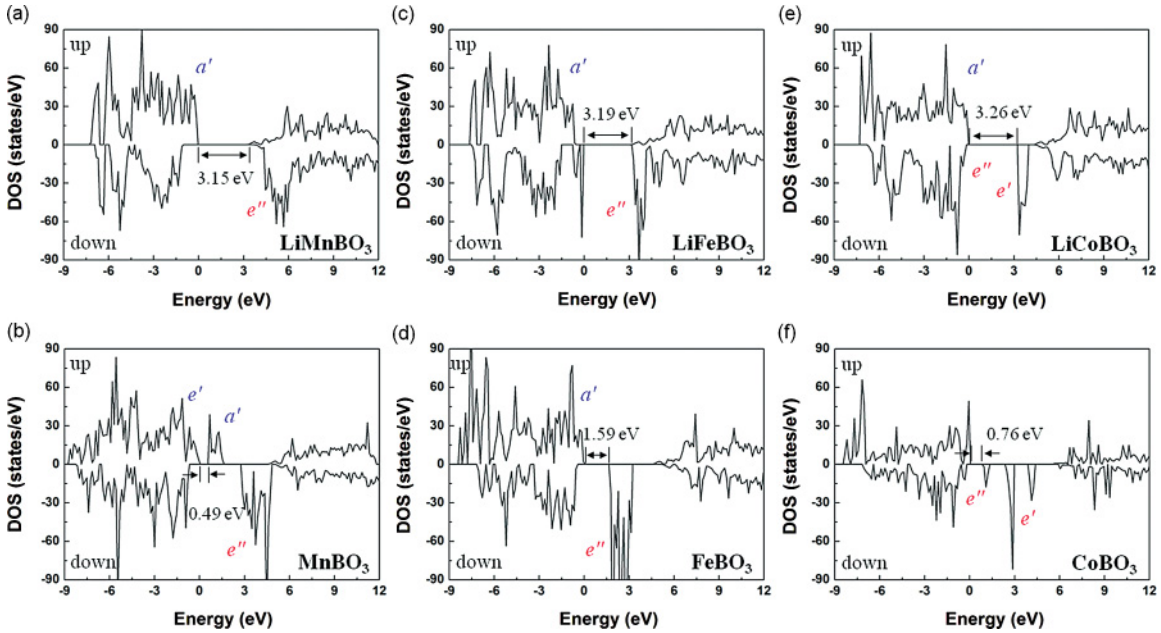

FIG. 3. (Color online) DOS of Li_xMBO_3 ($x = 1$, 0, M = Mn, Fe, Co). Highest occupied bands, lowest unoccupied bands, and bandgaps are presented.

occupy the e'', e', and a' bands, while one down-spin electron occupies the e'' band at a high-spin state. Thus both the highest occupied and the lowest unoccupied bands are for down-spin electrons, as shown in Fig. 3(c). Once the down-spin electron is extracted from the e'' band of $LiFeBO_3$ with delithiation, the highest occupied band becomes the a' band for the up-spin electron, as shown in the DOS of $FeBO_3$ [Fig. 3(d)]. Similarly, Figs. 3(e)–3(f) show that both the highest occupied and lowest unoccupied bands are for down-spin electrons in $LiCoBO_3$ and $CoBO_3$. Two down-spin electrons occupy the e'' band for $LiCoBO_3$, and one of these two electrons will be extracted with delithiation, as shown in Fig. 2(b).

The changes in the electronic structures are correlated with the structural evolution of Li_xMBO_3 with delithiation, as briefly mentioned above. When an Li ion is removed from $LiMnBO_3$, the electron in the highest occupied state band, a', will be extracted simultaneously. As the electron in the d_{z^2} orbital in the a' band is removed, the electrostatic repulsion with the oxygen $2p$ orbital along the z axis in Fig. 2 will be greatly relieved. Thus, the c lattice parameter which is parallel to the z axis of $MnBO_3$ reduces compared with that of $LiMnBO_3$. On the contrary, the delithiation extracts the electron from the orbital of the e'' band (d_{xz}, d_{yz}) which does not overlap with oxygen ions, as shown in Fig. 2 for $LiFeBO_3$ and $LiCoBO_3$. Therefore, a significant change in c lattice parameters does not occur.

The bandgaps of Li_xMBO_3 are also determined from the calculated DOS in Fig. 3. Table II lists the bandgaps of Li_xMBO_3 (M = Mn, Fe, and Co) at $x = 1$ and $x = 0$ with U_P. We note that calculated bandgaps of Li_xMBO_3 increase with U; therefore, care should be taken in consideration of the quantitative values of bandgaps. For $LiFeBO_3$, the bandgap is 3.190 eV at U_P, 2.970 eV at $U_P - 0.3$ eV, and 2.682 eV at $U_P - 0.6$ eV. However, it is noteworthy that the bandgaps of borates are generally smaller than those of olivines even though they were calculated with the same scheme and U.[27] The bandgaps of borates are still large enough to prevent the intrinsic generation of an electron or hole; thus the carrier concentration will be determined by Li deficiency. Therefore, it is expected that bandgaps do not play a significant role in the electronic conductivity of borates, similar to the way that bandgaps also do not play a significant role in the electronic conductivity of other insulating intercalation materials such as olivine phosphates.[27] Instead of thermal excitation of an electron or hole over the bandgap, the small polaron localized around a TM ion is likely to determine the electronic conductivity of borates, similar to olivine materials. A small polaron can be confirmed by the charge localization and the lattice distortion around a TM. After 1 of the 16 Li ions is removed from $LiFeBO_3$, the integrated spin density of one of the Fe ions becomes +4.24, whereas those of other Fe ions are still +3.75. Only this Fe ion is transformed from Fe^{2+} ($e''^{3}\, e'^{2}\, a'^{1}$) to Fe^{3+} ($e''^{2}\, e'^{2}\, a'^{1}$) and its average Fe–O bond length is reduced from 2.12 to 2.00 Å.

C. Calculated voltages

The calculated average voltages of Li_xMBO_3 (M = Mn, Fe, Co) vs. Li when applied to lithium batteries are discussed in this chapter. The method of calculating average voltages of electrode materials has been well established.[26,45–51] The average voltages can be obtained from:

$$\langle V \rangle = -[E(\mathrm{LiMBO_3}) - E(\mathrm{MBO_3}) - E(\mathrm{Li})] / F,$$

where E is the energy of the fully relaxed ground state structure and F is the Faraday constant. Figure 4 shows calculated average voltages of Li_xMBO_3. The average voltage of $LiFeBO_3$ calculated with GGA + U (3.02 V) is in agreement with experimental results (3.0 V).[15,18] In fact, the calculated average voltage without U (U = 0) resulted in a significantly underestimated value, reflecting the fact that $LiMBO_3$ is a strongly correlated system like $LiMPO_4$.[26] The systematic

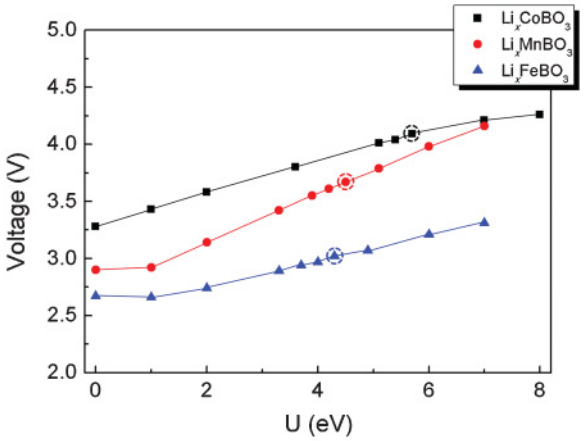

	$LiFeBO_3$	$LiMnBO_3$	$LiCoBO_3$
U_P	3.02 V	3.67 V	4.09 V
U_P-0.3 eV	2.97 V	3.61 V	4.04 V
U_P-0.6 eV	2.94 V	3.55 V	4.01 V

FIG. 4. (Color online) Calculated average voltages of Li_xMBO_3 (M = Mn, Fe, Co) vs. Li as functions of various U values. U_P values are U parameters of each TM ion in the olivine phosphate and indicated by dashed circles in the graph.

shift of average voltages among different TM ions in borates is also observed. The redox potentials of Mn^{2+}/Mn^{3+} and Co^{2+}/Co^{3+} were higher than those of Fe^{2+}/Fe^{3+}, resulting in higher average voltages by about 0.6 V and 1.1 V for $LiMnBO_3$ and $LiCoBO_3$, respectively, than for $LiFeBO_3$. The average voltages of the borates are calculated to be about 0.4V lower than those of the olivine phosphates reported by Zhou *et al.* using the same computational methods.[26] This is because B has a lower electronegativity than P (2.0 vs. 2.2), which leads to a weaker inductive effect for the polyanion.[20] The weaker inductive effect provided by B will increase the covalency of M–O in Li_xMBO_3. The strong covalency of M–O generally lowers the potential of a given M redox couple.[2,20] However, the differences in voltages among Li_xMBO_3 (M = Mn, Fe, Co) remain similar to those among Li_xMPO_4. This indicates that the change in inductive effect applies in a similar way for each TM system. The relatively low operation voltages of $LiMBO_3$ can be generally disadvantageous for practical purposes in terms of energy density. However, the theoretical capacity of $LiMBO_3$ is higher by about 50 mAh g^{-1} than that of $LiMPO_4$, and thus the theoretical energy density of $LiMBO_3$ can be 10% higher than that of $LiMPO_4$. Also, the voltages of $LiMnBO_3$ and $LiCoBO_3$ appear to be quite attractive for use as cathodes.

D. Li diffusion

Fast Li diffusion in a crystal structure of electrode materials is essential to the high-power capability of Li rechargeable batteries. In this sections, Li mobility in Li_xMBO_3 (M = Mn, Fe, Co) is investigated for a few plausible Li diffusion paths with the calculation of activation barriers. The most plausible diffusion path will be within the LiO_4 chains along the *c* direction in $LiMBO_3$, as shown in Figs. 1(b) and 4(a). The energies are plotted as a Li ion hops along this diffusion path in Fig. 5(b). There are two different activation barriers (A and B)

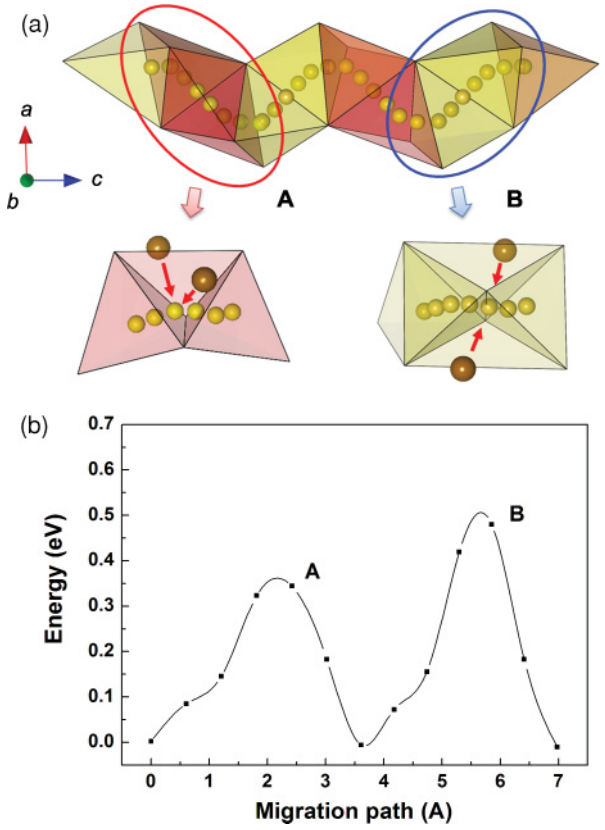

FIG. 5. (Color online) Trajectory and activation barrier of the Li hopping in the diffusion path along the *c* direction: (a) The transition state of A type (red) and the transition state of B type (yellow), and (b) their activation energies for Li diffusion along the *c* direction of $LiMBO_3$. Yellow circles indicate Li ions, and gold circles indicate TM ions, and the points of tetrahedrons are oxygen ions. Red arrows indicate the electrostatic repulsion between TM ions and Li ions.

repeatedly appearing as an ABAB sequence along the chain. The two activation barriers come from two symmetrically different types of Li hopping in the [001] chain. When the Li ion diffuses by means of type A edge-sharing, it hops from the original tetrahedral site to the other through the intermediate tetrahedral site, as shown in Fig. 5(a). At this intermediate site, the Li ion experiences the electrostatic repulsion from the neighboring two TM ions and, as a result, is slightly shifted off the center of the tetrahedron. This intermediate site acts as a first activation barrier for Li hopping. In the case of type B edge-sharing, two LiO_4 tetrahedrons share the edge with bisymmetry and yield to two intermediate tetrahedral sites above and below the shared edge, as shown in Fig. 5(a). However, a Li ion cannot move through either of these intermediate tetrahedral sites because of strong repulsion from the neighboring TM ions. The distance between the center of the intermediate tetrahedral site and the nearest TM ion is only about 2.06 Å (about 2.46 Å for type A), and thus the Li ion should move through the edge shared by two tetrahedrons in order to minimize the repulsion from TM ions. To pass across the edge of LiO_4, a Li ion should push out two oxygen ions of the edge (from 3.28 to 3.65 Å at the transition state), which results in a notably higher activation barrier in type B edge-sharing.

TABLE III. Activation barriers for Li diffusion in a LiO_4 chain of Li_xMBO_3 ($x \approx 1$, M = Mn, Fe, Co).

	A	B
Li_xMnBO_3	0.355	0.491
Li_xFeBO_3	0.223	0.437
Li_xCoBO_3	0.366	0.479

Table III shows activation barriers for Li motion along type A and type B edge-sharing for Li_xMBO_3 ($x \approx 1$, M = Mn, Fe, and Co). Activation barriers are about 300 meV for the A type and about 450 meV for the B type in Li_xMBO_3. Activation barriers of type B in Li_xMBO_3 are about 150 meV higher than those of type A since transition states of type B are less stable than those of type A, as explained above. Since Li ions should overcome both A and B activation barriers to diffuse along the [001] direction, hopping through the type B barrier is likely to be a rate-limiting step for Li mobility. Therefore, the activation barriers for the type B path should be considered a activation barriers for Li diffusion. It appears that these activation barriers are higher than those of conventional cathode materials such as spinel, olivine, and layered cathode materials calculated within similar schemes. Morgan *et al*. reported that the Li activation barriers in olivine electrodes are about 300 meV.[34] Kang and Ceder reported that the Li activation barrier in $LiCoO_2$ is about 250 meV.[35,52] Ma *et al*. recently reported that the Li activation barrier in a $LiNi_{0.5}Mn_{1.5}O_4$ spinel structure is about 350 meV.[36] Those values are about 100 meV lower than the observed value in $LiMBO_3$. The diffusion constant can be estimated as

$$D = a^2 \nu^* \exp(-E_{act}/k_B T),$$

where ν^* is the attempt frequency and E_{act} is the activation barrier for the hop.[30,34] Assuming that ν^* is about 10^{12} Hz, which is generally in the range of phonon frequencies,[34] and a is approximately 3 Å, corresponding to the distance of a hop along the [001] direction, the diffusion constant of Li_xMBO_3 can be approximated to be 10^{-11} cm^2 s^{-1} at room temperature. Assuming the same prefactor of diffusivity, Li diffusivity in borates is expected to be lower by 2 orders of magnitude than those of conventional cathodes.[34–36,52]

Another potential diffusion path is hopping between LiO_4 chains, as shown in Fig. 6. To hop to the neighboring chain, a Li ion should pass through the distorted octahedral site which face-shares with two MO_5. This transition state appears to be energetically unstable due to the strong electrostatic repulsion from closely located TM ions. The calculated activation barrier of this path is about 1.5 eV for Li_xMBO_3 ($x \approx 1$, M = Mn, Fe, and Co), implying that Li ions are not likely to cross between LiO_4 chains. Hence, it is expected that $LiMBO_3$ is a 1D lithium diffuser like olivine electrode materials.

Electrode materials with 1D Li diffusion are sensitive to the presence of defects in the diffusion channel.[34,53–55] When defects block the diffusion channel, Li must detour through paths with high activation barriers, and the power capability of the electrode is therefore greatly reduced. One of the most plausible intrinsic defects is the antisite defect which is the interchange of sites between Li ions and TM ions. Islam *et al*.[53] and Fisher *et al*.[54] determined by atomic simulation techniques

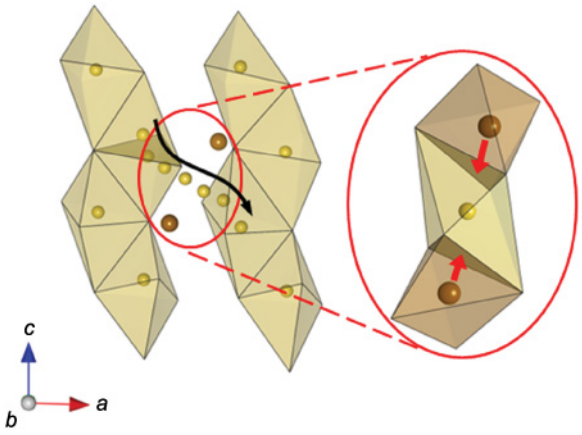

FIG. 6. (Color online) Li diffusion between LiO_4 chains. The transition state of Li diffusion is highlighted in the red circle. Yellow circles indicate Li ions, and gold circles indicate TM ions. Red arrows indicate the electrostatic repulsion between TM ions and Li ions.

that the antisite energy of $LiFePO_4$ is about 740 meV. Malik *et al*. determined through first-principles calculation that the antisite energy of $LiFePO_4$ is about 550 meV.[55] Chung *et al*. also experimentally observed around 1% of the disorder between Li and Fe ions with scanning transmission electron microscopy (STEM).[56] Even the presence of a low percentage of antisite defects in $LiFePO_4$ can significantly reduce the Li mobility to block a 1D diffusion path.[34,53–55] Since the antisite defects are critical to Li mobility in materials with 1D diffusion channels, we performed a preliminary calculation on the antisite energies in $LiMBO_3$. The antisite energy is evaluated by taking the energy difference between the original structure and the structure with a pair of antisite Li and TM ions. The results are 747 meV for $LiMnBO_3$ and 549 meV for $LiFeBO_3$. At typical solid-state synthesis temperatures (900–1100 K), the antisite defect concentrations of these borate materials are about 0.01%–0.3%, which are similar to these of $LiFePO_4$ calculated within the same computational scheme.[55] Relatively small antisite energies of $LiMBO_3$ are rather unexpected, since the antisite defects usually form between two ions with similar size and coordination.[54] Li occupies tetrahedral sites, while TM is in trigonal bipyramidal sites in $LiMBO_3$. Further study on the antisite defect in borates is ongoing and will be published elsewhere. These low antisite energies can induce disorder within Li diffusion channels, and can thus present a critical kinetics problem. Therefore, efforts should be made to prevent the formation of the antisite defect of borates at the synthesis level. Also, as recently found, nano-sizing can be effective to minimize the influence of the blockage of channels by defects.[55]

IV. CONCLUSIONS

A computational study of the structural, electronic, and electrochemical properties of lithium metal borates as cathode materials is conducted using a first-principles calculation. Small volume changes of Li_xMBO_3 (M = Mn, Fe, Co) with delithiation were confirmed, and these changes may facilitate decalation or intercalation with high reversibility. The calculated DOS indicates that Li_xMBO_3 can be polaronic conductors similar to olivine phosphates. The average voltages

of Li_xMBO_3 were predicted to be lower than those of Li_xMPO_4 by about 0.4 V. Li_xMBO_3 appears to be a 1D Li diffuser with a reasonably low activation barrier. However, in comparison with those reported for olivine, spinel, and layered structures, the Li diffusivity is expected to be lower by about 2 orders of magnitude. In addition, the high probability of antisite defects of Li_xMBO_3 may be disadvantageous for high-power capability.

ACKNOWLEDGMENTS

This research was supported by the Converging Research Center Program through the Ministry of Education, Science and Technology (2010K001088) and the Fundamental R&D Program for Technology of World Premier Materials funded by the Ministry of Knowledge Economy, Republic of Korea. The authors are grateful to KISTI (Grant No. KSC-2009-S03-0011) for providing supercomputing resources.

*matlgen1@snu.ac.kr

[1] A. K. Padhi, K. S. Nanjundaswamy, C. Masquelier, S. Okada, and J. B. Goodenough, J. Electrochem. Soc. **144**, 1609 (1997).
[2] A. K. Padhi, K. S. Nanjundaswamy, and J. B. Goodenough, J. Electrochem. Soc. **144**, 1188 (1997).
[3] A. Yamada, S. C. Chung, and K. Hinokuma, J. Electrochem. Soc. **148**, A224 (2001).
[4] S.-W. Kim, J. Kim, H. Gwon, and K. Kang, J. Electrochem. Soc. **156**, A635 (2009).
[5] H. Gwon, D.-H. Seo, S. W. Kim, J. Kim, and K. Kang, Adv. Funct. Mater. **19**, 3285 (2009).
[6] D.-H. Seo, H. Gwon, S.-W. Kim, J. Kim, and K. Kang, Chem. Mater. **22**, 518 (2010).
[7] J. Kim, D.-H. Seo, S.-W. Kim, Y.-U. Park, and K. Kang, Chem. Commun. **46**, 1305 (2010).
[8] Y.-U. Park, J. Kim, H. Gwon, D.-H. Seo, S.-W. Kim, and K. Kang, Chem. Mater. **22**, 2573 (2010).
[9] G. Arnold, J. Garche, R. Hemmer, S. Strobele, C. Vogler, and M. Wohlfahrt-Mehrens, J. Power Sources **119–121**, 247 (2003).
[10] A. Nytén, A. Abouimrane, M. Armand, T. Gustafsson, and J. O. Thomas, Electrochem. Commun. **7**, 156 (2005).
[11] M. E. Arroyo-de Dompablo, M. Armand, J. M. Tarascon, and U. Amador, Electrochem. Commun. **8**, 1292 (2006).
[12] N. Kuganathan and M. S. Islam, Chem. Mater. **21**, 5196 (2009).
[13] B. L. Ellis, W. R. M. Makahnouk, Y. Makimura, K. Toghill, and L. F. Nazar, Nat. Mater. **6**, 749 (2007).
[14] N. Recham, J. N. Chotard, L. Dupont, C. Delacourt, W. Walker, M. Armand, and J. M. Tarascon, Nat. Mater. **9**, 68 (2010).
[15] V. Legagneur, Y. An, A. Mosbah, R. Portal, A. Le Gal La Salle, A. Verbaere, D. Guyomard, and Y. Piffard, Solid State Ionics **139**, 37 (2001).
[16] A. Abouimrane, M. Armand, and N. Ravet, in *New Trends in Intercalation Compounds for Energy Storage and Conversion: Proceedings of the International Symposium* (Electrochemical Society, New York, 2003), p. 15.
[17] Y. Z. Dong, Y. M. Zhao, Z. D. Shi, X. N. An, P. Fu, and L. Chen, Electrochim. Acta **53**, 2339 (2008).
[18] A. Yamada, N. Iwane, Y. Harada, S.-I. Nishimura, Y. Koyama, and I. Tanaka, Adv. Mater. **22**, 3583 (2010).
[19] Y. Koyama, I. Tanaka, N. Iwane, S. Nishimura, and A. Yamada, *ECS Meeting Abstracts*, **1003**, 480 (2010).
[20] A. K. Padhi, K. S. Nanjundaswamy, C. Masquelier, and J. B. Goodenough, J. Electrochem. Soc. **144**, 2581 (1997).
[21] S. P. Ong, L. Wang, B. Kang, and G. Ceder, Chem. Mater. **20**, 1798 (2008).
[22] S. P. Ong, A. Jain, G. Hautier, B. Kang, and G. Ceder, Electrochem. Commun. **12**, 427 (2010)
[23] J. P. Perdew, K. Burke, and M. Ernzerhof, Phys. Rev. Lett. **77**, 3865 (1996).
[24] G. Kresse and J. Furthmuller, Comput. Mater. Sci. **6**, 15 (1996).
[25] K. Kang, C. H. Chen, B. J. Hwang, and G. Ceder, Chem. Mater. **16**, 2685 (2004).
[26] F. Zhou, M. Cococcioni, C. A. Marianetti, D. Morgan, and G. Ceder, Phys. Rev. B **70**, 235121 (2004).
[27] F. Zhou, K. S. Kang, T. Maxisch, G. Ceder, and D. Morgan, Solid State Commun. **132**, 181 (2004).
[28] K. Kang, Y. S. Meng, J. Breger, C. P. Grey, and G. Ceder, Science **311**, 977 (2006).
[29] J. Breger, Y. S. Meng, Y. Hinuma, S. Kumar, K. Kang, Y. Shao-Horn, G. Ceder, and C. P. Grey, Chem. Mater. **18**, 4768 (2006).
[30] K. Kang, D. Morgan, and G. Ceder, Phys. Rev. B **79**, 014305 (2009).
[31] J. L. F. Da Silva, M. V. Ganduglia-Pirovano, J. Sauer, V. Bayer, and G. Kresse, Phys. Rev. B **75**, 045121 (2007).
[32] V. I. Anisimov, J. Zaanen, and O. K. Andersen, Phys. Rev. B **44**, 943 (1991).
[33] V. I. Anisimov, F. Aryasetiawan, and A. I. Lichtenstein, J. Phys.Condens. Matter **9**, 767 (1997).
[34] D. Morgan, A. Van der Ven, and G. Ceder, Electrochem. Solid State Lett. **7**, A30 (2004).
[35] K. Kang and G. Ceder, Phys. Rev. B **74**, 094105 (2006).
[36] X. Ma, B. Kang, and G. Ceder, J. Electrochem. Soc. **157**, A925 (2010).
[37] H. Jonsson, G. Mills, K. W. Jacobsen, and B. J. Berne, in *Classical and Quantum Dynamics in Condensed Phase Simulations*, edited by D. Chandler, B. J. Berne, G. Ciccotti, and D. F. Coker (World Scientific, Singapore, 1998), p. 385.
[38] S. Curtarolo, D. Morgan, and G. Ceder, Calphad **29**, 163 (2005).
[39] Y. Piffard, K. K. Rangan, Y. An, D. Guyomard, and M. Tournoux, Acta Crystallogr. C **54**, 1561 (1998).
[40] O. S. Bondareva, M. A. Simonov, Y. K. Egorov-Tismenko, and N. V. Belov, Sov. Phys. Crystallogr. **23**, 269 (1978).
[41] H. Berg and J. O. Thomas, Solid State Ionics **126**, 227 (1999).
[42] J. Reed, G. Ceder, and A. Van der Ven, Electrochem. Solid-State Lett. **4**, A78 (2001).
[43] B. J. Hwang, Y. W. Tsai, D. Carlier, and G. Ceder, Chem. Mater. **15**, 3676 (2003).
[44] A. E. Smith, H. Mizoguchi, K. Delaney, N. A. Spaldin, A. W. Sleight, and M. A. Subramanian, J. Am. Chem. Soc. **131**, 17084 (2009).

[45]A. Van der Ven and G. Ceder, Phys. Rev. B **59**, 742 (1999).
[46]F. Zhou, M. Cococcioni, K. Kang, and G. Ceder, Electrochem. Commun. **6**, 1144 (2004).
[47]G. Ceder, Y. M. Chiang, D. R. Sadoway, M. K. Aydinol, Y. I. Jang, and B. Huang, Nature (London) **392**, 694 (1998).
[48]G. Ceder, Science **280**, 1099 (1998).
[49]M. K. Aydinol, A. F. Kohan, G. Ceder, K. Cho, and J. Joannopoulos, Phys. Rev. B **56**, 1354 (1997).
[50]M. K. Aydinol, A. F. Kohan, and G. Ceder, J. Power Sources **68**, 664 (1997).
[51]Y. S. Meng and M. E. A.-D. Dompablo, Energy Environ. Sci. **2**, 589 (2009).
[52]A. Van der Ven, G. Ceder, M. Asta, and P. D. Tepesch, Phys. Rev. B **64**, 184307 (2001).
[53]M. S. Islam, D. J. Driscoll, C. A. J. Fisher, and P. R. Slater, Chem. Mater. **17**, 5085 (2005).
[54]C. A. J. Fisher, V. M. Hart Prieto, and M. S. Islam, Chem. Mater. **20**, 5907 (2008).
[55]R. Malik, D. Burch, M. Bazant, and G. Ceder, Nano Lett. **10**, 4123 (2010).
[56]S.-Y. Chung, S.-Y. Choi, T. Yamamoto, and Y. Ikuhara, Phys. Rev. Lett. **100**, 125502 (2008).